Mon. Not. R. Astron. Soc. **000**, 1–9 (1999) Printed 24 August 1999 (MN LATEX style file v1.4)

Infrared emission from 6.7-GHz methanol maser sources

S. Goedhart[1,2] ⋆, D. J. van der Walt[1] and A. J. Schutte[3,4]

[1] *Space Research Unit, Physics Department, Potchefstroom University for CHE, Private Bag X6001, Potchefstroom, 2520, South Africa*
[2] *Current address: Hartebeesthoek Radio Astronomy Observatory, PO Box 443, Krugersdorp, 1740, South Africa,*
[3] *Department of Physics, University of Zululand, Kwadlangezwa, 3886, South Africa*
[4] *Current affiliation: Vodacom, South Africa*

Accepted 1999; Received 1999; in original form 1999

ABSTRACT

Near-infrared photometry was done on 56 southern 6.7 GHz methanol maser sources. A simple spherically symmetric model of the radiative transfer through a dust shell was developed and used to study the conditions in the dust cloud in which the masers are produced. The parameters investigated were the size of the cloud, the spectral type of the embedded star, the optical depth of the dust cloud and the dust density distribution. It was found that the infrared colours of the models have a complex dependence on the parameters and that no unique combination of parameter values explains the spectral energy distribution of any particular source. The model effectively reproduces the far-infrared (*IRAS*) colours but cannot simultaneously explain the near-infrared colours for any of the observed sources.

Key words: masers – HII regions – ISM: clouds – Radio lines: ISM

1 INTRODUCTION

Studying the very early phases of massive stars is not an easy task. Massive stars are generally formed deeply embedded in giant molecular clouds and therefore cannot be observed optically. However, the profound effect of massive stars on the interstellar medium (Leitherer et al. 1992) requires that massive stars be studied in detail if the evolution of the Galaxy is to be understood.

The energy input from the young massive stars into their immediate environment often leads to masing of hydroxyl, water and methanol molecules. The 6.7-GHz methanol maser transition has proven to be very useful in tracing regions of star formation since these masers are strong and widespread in the Galaxy (Menten 1991; Caswell 1996, and references therein). To date, over 400 individual sources have been detected. The exact nature of these maser sources is unclear at present. It has been assumed that the sources are associated with recently formed massive stars because many of the masers are associated with OH masers and ultracompact (UC) HII regions (Caswell 1996). Although radio free-free emission has been detected towards many methanol maser sources, indicating the presence of an ionizing star, there are a number of methanol maser sources for which no radio or infrared counterparts have been found (Phillips et al. 1998). It is not clear whether the absence of radio free-free and infrared counterparts in some cases is a sensitivity effect, an evolutionary effect or whether the masers are also associated with lower mass stars (Phillips et al. 1998). Resolving this problem requires more sensitive measurements in the radio and near-infared (NIR).

Most of the energy radiated from the embedded star emerges as infrared emission from the dust surrounding the star. As the radiation propagates through the dust cloud, it is shifted through repeated absorption and reemission to longer wavelengths, until the radiation emerging is predominantly far-infrared (FIR). The Infrared Astronomical Satellite (*IRAS*) Point Source Catalog (PSC) has proven to be very useful in identifying different types of objects based on their far-infrared (FIR) colours. Deeply embedded young stellar objects also have specific infrared colours which can be used to determine which *IRAS* sources are likely to be UC HII regions (Wood & Churchwell 1989b).

Numerous models of radiative transfer through dust clouds have been developed in the past to explain the spectral energy distributions (SEDs) of embedded low and high mass stars. One of the earliest models was developed by Scoville & Kwan (1976) who computed the temperature gradients across the dust cloud by solving the equation of radiative equilibrium. More sophisticated models, in which the equation of radiative transfer is solved directly and which involve fewer approximations, have also been applied to star formation regions (Yorke 1980; Rowan-Robinson 1980; Crawford & Rowan-Robinson 1986; Wolfire & Cassinelli 1986, for example). All of the models mentioned above assume a spherically symmetric dust cloud. Axisymmetric dust clouds have also been modelled to investigate the effects of circumstellar disks (Yorke et al. 1995; Kenyon

⋆ E-mail: sharmila@bootes.hartrao.ac.za

et al. 1993; Efstathiou & Rowan-Robinson 1990; Kessel et al. 1998, for example). Results from these models indicate that the presence of a circumstellar disk does have a significant effect on the SED at NIR wavelengths. However, these disk models have not been applied to massive star formation regions.

The aim of this work is to report on the NIR observations of 6.7 GHz methanol maser sources and to use a simple model of radiative transfer through the dust shell to help interpret the results. Up to now, the infrared characteristics of 6.7 GHz methanol maser sources have not been studied in detail. The observations will be described in Section 2 and the results will be presented in Section 3. In Section 4 we model the infrared colours of 6.7 GHz methanol masers. We use an approximate method (described in Appendix A) based on the method described by Scoville & Kwan (1976) which nonetheless compares well with the results from the more advanced spherically symmetric models discussed above. A sample of the results of a parameter study investigating the effect of the size and optical depth of the surrounding dust cloud, the dust density distribution and the spectral type of the central star are presented. A brief discussion of the implications of the parameter study is given in section 5.

2 THE OBSERVATIONS

The 1.9m telescope of the South African Astronomical Observatory (SAAO) at Sutherland was used with the Mk III infrared photometer. The first observations were made during the week of 18–24 May 1993 and the second during 24–30 May 1994. Sources were selected from 6.7-GHz methanol masers known at that time (Menten 1991; MacLeod et al. 1992; MacLeod & Gaylard 1992; van der Walt et al. 1995; Schutte et al. 1993) for which unique *IRAS* counterparts could be identified and which could be observed from Sutherland. No other selection criteria were applied to the maser sources. The detection limit was about 12^m in K-band. The standard procedures applicable to NIR observing on the 1.9m telescope at SAAO were followed, which included the regular observation of standard stars during the night. Observations were made on photometric nights only.

For each source the associated *IRAS* error ellipse was scanned in K-band with a diaphragm of 18 arcsec. Since such a large aperture can lead to confusion, densely populated regions (e.g. towards the Galactic center) were avoided. Although in many cases only a single bright K-band source was found in the *IRAS* error ellipse, in other cases two or three sources were found. Broad band photometry was then done on all the sources in the error ellipse.

The data were reduced at SAAO using the standard SAAO data reduction software. The errors on the derived magnitudes were typically less than one percent.

3 OBSERVATIONAL RESULTS

The results of the broad band photometry are given in Table 1. Flux densities from the *IRAS* PSC (1985) were used to examine the behavior of the SEDs at FIR wavelengths. There were fourteen cases where more than one NIR source

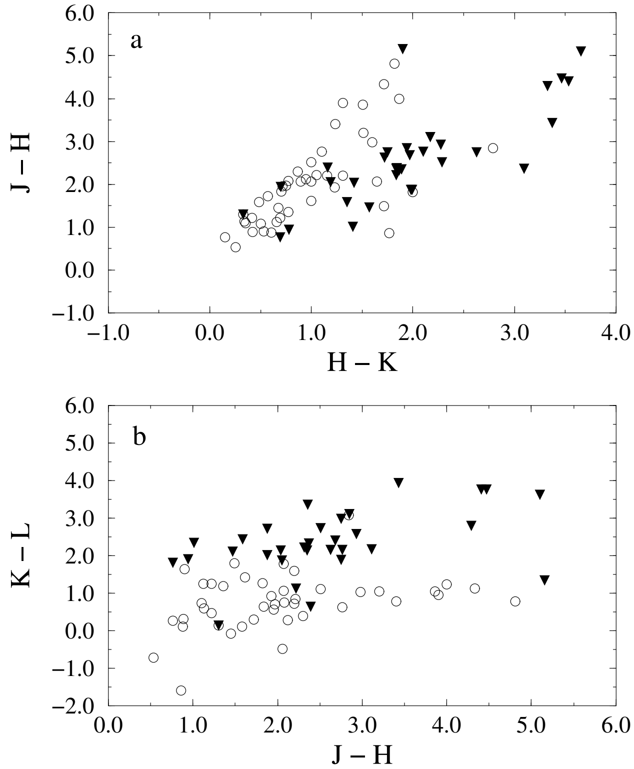

Figure 1. Infrared two-colour diagrams. a) [J−H] vs [H−K] diagram. b) [K−L] vs [J−H] diagram. The sources have been subdivided according to whether they possess the inflection feature shown in Fig. 2b. The open circles represent the sources with the inflection feature while the filled triangles represent the sources with smooth SEDs. The observed sources will be represented in the same way in all of the following NIR 2-colour diagrams.

was found in the *IRAS* error ellipse. At this stage it is not possible to determine which source is associated with the maser. For the purposes of this paper, the NIR colours of all the sources in the error ellipse will be considered. Four of the sources, 10460-5811, 13395-6153, 18060-2005 and 18449-0158, had varied when they were re-observed in 1994. All the observations are used in this study, but the variable sources require further investigation. Comparison of observations of the methanol masers taken at different epochs by different investigators shows that the methanol maser strengths are also variable for 10460-5811 (van der Walt et al. 1995; Caswell et al. 1995) and 13395-6153 (MacLeod et al. 1992; Caswell et al. 1995). Simultaneous monitoring at 6.7-GHz and the NIR will be necessary to determine whether the variability in the NIR and radio are correlated.

Since it is impractical to show the SED of every individual source, we present our results as two-colour diagrams. Fig. 1 shows the NIR colours of the maser sources. The NIR colours cover a remarkably large range. This is mainly because there are large differences in the shapes of the SEDs in the NIR. Closer inspection shows that there are basically two groups of SEDs viz. those which increase monotonically from J-band up to 100 μm and those which show an inflection around L-band (57 % of the sources). In Fig. 2 we show the SEDs of two sources as representative examples of the two groups. The source 13471-6120 has a SED which

Table 1. Infrared magnitudes of observed sources. Sources with an 'A' or 'B' appended to the IRAS name indicate that multiple sources were found in the *IRAS* error box. Some sources were found to be variable when they were re-observed. Five sources were too faint to be observed at J band and two others were too faint at L-band. Sources marked with an * have an inflection in the SED near the L-band.

IRAS name	J	H	K	L	Year	*IRAS* name	J	H	K	L	Year
08470-4243	11.110	10.350	9.657	7.844	1993	16297-4757*	12.650	10.580	9.685	8.626	1994
10295-5746*	10.760	9.880	9.275	9.172	1993	16313-4840*	11.780	10.560	9.867	8.618	1993
10303-5746	13.520	11.010	8.723	5.988	1994	16374-4701A*	12.870	10.800	9.156	7.386	1994
10460-5811	11.550	9.170	7.346	5.018	1994	16374-4701B*	10.480	9.400	8.904	—	1994
10460-5811	11.470	9.150	7.289	5.080	1994	16465-4437	13.870	11.480	10.320	9.690	1994
10460-5811	11.820	9.460	7.583	5.453	1993	16477-4408*	11.560	8.790	7.694	7.081	1994
11097-6102*	11.670	10.180	8.467	6.683	1994	16586-4142A	13.590	10.960	9.242	7.094	1993
11368-6312	13.990	12.400	11.050	8.623	1993	16586-4142B	13.330	10.950	9.109	—	1993
12320-6122A*	8.990	8.230	8.083	7.826	1993	17008-4040*	13.210	11.010	9.702	8.123	1994
12320-6122B*	9.840	9.310	9.058	9.792	1993	17158-3901	13.050	11.000	9.809	7.942	1994
13079-6218	14.040	11.110	8.834	6.257	1994	17200-3658	14.650	12.770	10.790	8.777	1993
13080-6229*	12.220	11.090	10.750	10.170	1994	17271-3439	13.550	12.080	10.510	8.415	1994
13374-6130A*	11.900	10.780	10.120	8.874	1994	17425-2921A	12.920	10.880	9.460	7.324	1994
13374-6130B*	14.630	12.810	10.810	9.552	1994	17425-2921B*	10.880	9.970	9.451	7.816	1994
13395-6153	14.230	9.820	6.285	2.533	1994	17430-2822	—	13.440	9.250	7.576	1993
13395-6153	14.440	9.960	6.504	2.751	1994	17470-2853	12.690	11.750	10.970	9.076	1994
13395-6153	15.090	9.990	6.338	2.721	1993	17577-2320	—	11.960	10.540	9.866	1993
13471-6120	14.090	11.340	8.713	5.733	1994	17577-2320A*	12.330	11.470	9.705	11.310	1993
14212-6131*	11.870	9.940	8.717	7.807	1993	17577-2320B	—	11.330	9.499	8.080	1993
14394-6004*	12.630	10.330	9.462	9.085	1994	18060-2005*	11.490	9.270	8.229	7.398	1994
14416-5937A*	15.830	11.020	9.204	8.432	1994	18060-2005	11.660	9.460	8.313	7.604	1993
14416-5937B*	14.390	10.390	8.528	7.294	1994	18060-2005A*	15.890	11.560	9.844	8.719	1993
15061-5814*	11.970	9.890	9.121	8.384	1994	18060-2005B*	14.120	11.140	9.539	8.508	1994
15122-5801A*	9.270	7.970	7.640	7.501	1993	18075-1956*	13.330	10.130	8.617	7.575	1994
15122-5801B	15.380	12.530	10.590	7.484	1993	18151-1208	14.280	11.920	8.826	5.470	1994
15254-5621*	13.670	10.830	8.044	4.980	1993	18196-1331	13.910	10.480	7.107	3.177	1993
15278-5620A*	11.970	10.610	9.839	8.662	1994	18319-0834	14.050	8.890	6.990	5.659	1994
15278-5620B*	11.680	10.580	10.230	9.498	1994	18379-0500*	14.000	10.600	9.363	8.584	1994
15394-5358	16.060	11.770	8.442	5.659	1993	18416-0420	12.000	9.230	7.130	4.975	1994
15408-5356*	10.760	9.140	8.147	6.727	1993	18434-0242	12.960	10.280	8.310	5.908	1993
15557-5215	—	13.240	11.630	10.310	1993	18449-0158*	9.704	7.860	7.161	6.532	1993
15557-5215	13.960	11.740	9.905	8.780	1993	18449-0158	9.744	7.780	7.075	6.512	1994
15579-5303A*	11.720	10.140	9.656	9.561	1994	18487-0015A*	14.040	10.140	8.831	7.879	1994
15579-5303B*	12.050	10.330	9.758	9.465	1994	18487-0015B*	12.920	10.800	9.852	9.584	1994
15584-5230*	14.370	10.510	9.002	7.957	1994	18592+0108	14.060	11.310	9.561	7.677	1994
16076-5134*	15.040	12.530	11.530	10.430	1994	19111+1048	11.530	9.650	7.657	4.938	1993
16085-5138A*	12.040	10.590	9.914	9.999	1994	19117+1107A*	11.540	10.320	9.903	9.436	1994
16085-5138B*	13.580	11.520	10.520	11.010	1994	19117+1107B*	11.320	9.350	8.605	7.911	1994
16172-5028A*	—	12.480	9.633	6.887	1993	19120+1103	14.790	11.680	9.511	7.353	1993
16172-5028B	7.739	6.850	6.427	6.125	1993						

increases monotonically from the NIR to the FIR. 13080-6229 is an example of the second group. In this case it is seen that the inflection at L-band extends to the K-band. In some cases it even affects the H-band flux density. It is not known whether we are seeing a strong absorption feature or the superposition of two quasi-blackbodies with different temperatures. Due to the fact that none of the maser sources have an optical counterpart, the possibility exists that the wrong source was observed in the NIR. However, it is highly unlikely that all the "wrong" sources have the same general behaviour in the NIR. It is worth noting that a similar feature can also be seen in the independently measured SEDs of the UC HII regions G19.61-0.23, G45.12+0.13 (Faison et al. 1998) and the compact HII regions G32.806+0.192 and G10.477+0.024 (Efstathiou & Rowan-Robinson 1994).

4 MODEL PREDICTIONS AND COMPARISON WITH OBSERVATIONS

To interpret the observed colours of the maser sources we developed a model for the radiative transfer in a spherical dust cloud with an embedded massive star at the centre of the cloud. The details of the calculational procedure are given in the Appendix.

Although the parameter space was surveyed extensively using the model, it is not possible to present all the results here. Rather, we will concentrate on a few results which highlight the essential model predictions in comparison with the observations.

The free parameters in the model were the following: the inner and outer radii of the dust cloud (r_i and r_o), the spectral type of the central star, the optical depth at 100μm ($\tau_{100\mu m}$) between the outer and inner radii, and the radial dust density distribution ($n_d(r) \propto r^{-\alpha}$). The inner radius

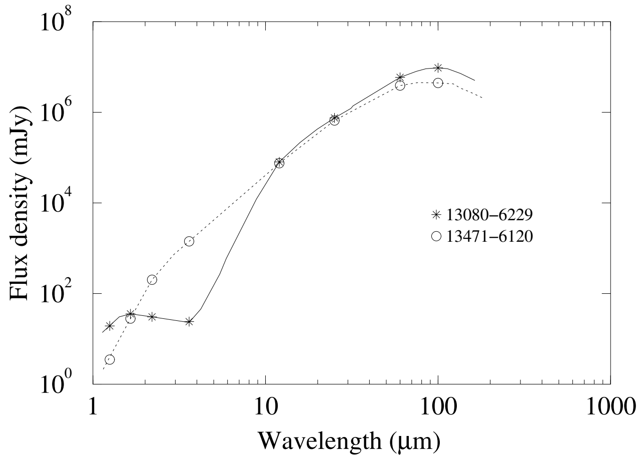

Figure 2. Typical SEDs represented by two sources. 13471-6120 has a smooth SED but 13080-6229 has an inflection in the region of L-band.

was determined by the dust destruction temperature (T_d) which was taken to be 1000 K in all the cases discussed here. The inner radius also depends on the spectral type of the star. The outer radius was generally taken to be equal to 1000 times the dust destruction radius. For the spectral type of the central star we considered types O4, O8 and B3, with the stellar parameters taken from Panagia (1973).

Only a single grain size is considered in the model, but the emissivity function used is averaged over a range of dust grain sizes. A more rigorous treatment would consider multiple dust grain sizes explicitly and is expected to give somewhat different results. The inclusion of very small dust grains, for example, will lead to an increase in the NIR emission (Siebenmorgen 1993). However, considering the agreement with the results from more sophisticated models (see Appendix), we believe that the results obtained with the model are sufficiently realistic that they can usefully be compared with the observations.

We compare the observations with the model predictions on two-colour diagrams in order to see what range of parameter values might explain the observations. The model SEDs were convolved with the filter response function of the NIR and IRAS filters before the colours were calculated. Model calculations were made for ten optical depths spaced at equal logarithmic intervals for $\tau_{100\mu m}$ between 0.05 and 0.5 ($\tau_{0.55\mu m} = 19$ to 192).

It was found that the model reproduced the scaling effect noted by Rowan-Robinson (1980) and Ivezić & Elitzur (1997). As a result, the colours are largely independent of the spectral type of the central star if the inner radius of the dust cloud is defined as the dust destruction radius and the outer radius is scaled with the inner radius. Therefore the results presented here will only be for an O4 type star.

The model prediction of the dependence of the infrared colours on the inner radius is shown in Fig. 3, where it is compared with the observed colours. The lines in each of the three panels are the model results whereas the open circles and filled triangles are the observed colours. For the model results, $\tau_{100\mu m}$ increases from 0.05 at the lower left hand point of each line to 0.5 at the upper right hand point of the line. The outer radius was kept fixed at 1000 times the dust destruction radius. A constant dust density law was assumed. The values of the inner radius (in terms of the dust destruction radius) are given in the figure. On examination of the [100−60]† *vs* [60−25] two colour diagram it is seen that the [100−60] colours are fairly insensitive to variations of the inner radius or the optical depth. The [60−25] colours are, however, strongly dependent on the optical depth. Fig. 3b shows that the [25−12] colours are fairly strongly dependent on the inner radius. The basic reason for this difference is that in the spherically symmetric model the 100 μm and 60 μm emission are predominantly produced close to the outer edge of the cloud (see Appendix). The 25 μm and 12 μm emission are, on the other hand, produced closer to the inner radius and are therefore more affected by the conditions at the inner edge than the longer wavelengths.

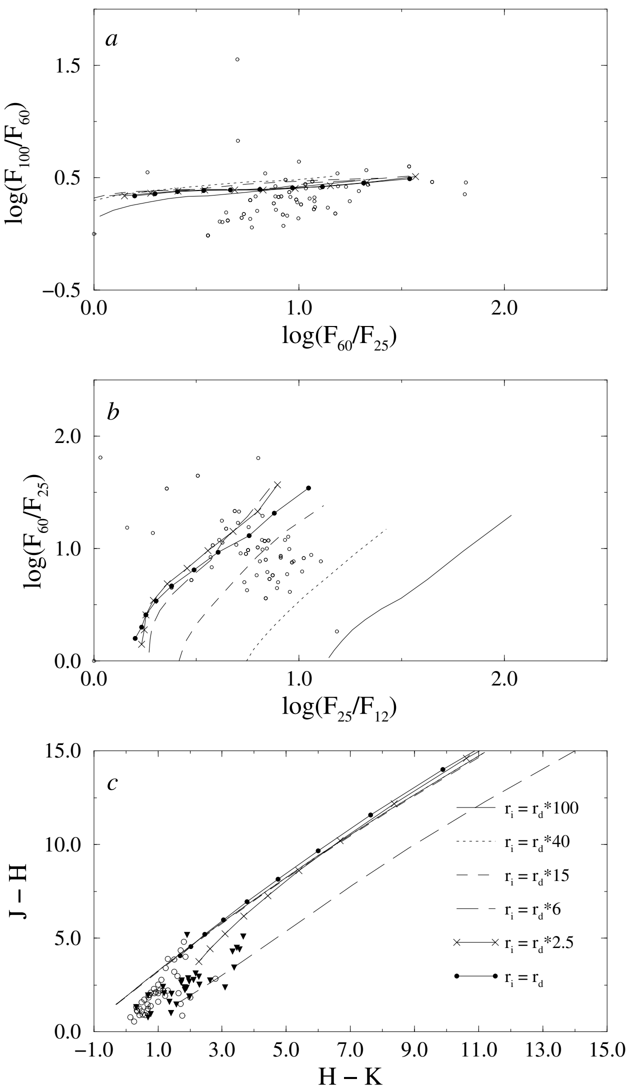

Figure 3. The effect of changing the inner radius. The central star has been set to spectral type O4 and the dust density distribution is constant. The dust destruction radius is $r_d = 1.27\times10^{14}$m.

† The notation $[\lambda_1 - \lambda_2]$ will serve as shorthand for $\log(F_{\lambda_1}/F_{\lambda_2})$.

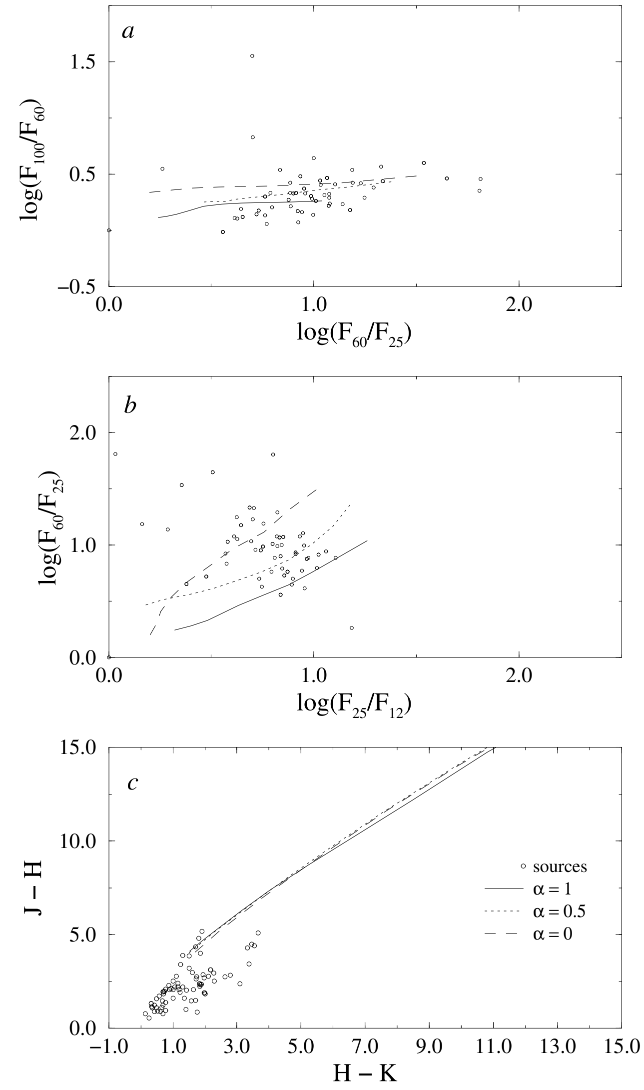

Figure 4. The effect of changing the dust density gradient. The density is expressed as $n_d(r) \propto r^{-\alpha}$.

There are a number of sources at the upper left of this diagram which fall outside the area bracketed by the model results. It will be seen that none of the models discussed here explain the colours of those sources. However, the distribution of the colours of the majority of the sources on the [60−25] *vs* [25−12] two-colour diagram can be explained by the range of optical depths and inner radii considered.

In the [J−H] *vs* [H−K] diagram (Fig. 3c) it is seen that the observations are bracketed by the model results. Inspection of Fig. 3c shows that the curve representing the models for $r_i = 6 * r_d$ is substantially offset from the other models. More detailed investigations have shown that this effect seems to due to increased emission at 9.7 μm when the temperature of the dust at the inner radius reaches certain temperatures. It it not clear whether this is an artifact of the simplifying assumptions made in this model or if it is significant physically.

The effect on the colours of changing the radial density gradient of the dust is shown in Fig. 4. Except for the radial density law, which now goes as $n_d(r) \propto r^{-\alpha}$ and the inner

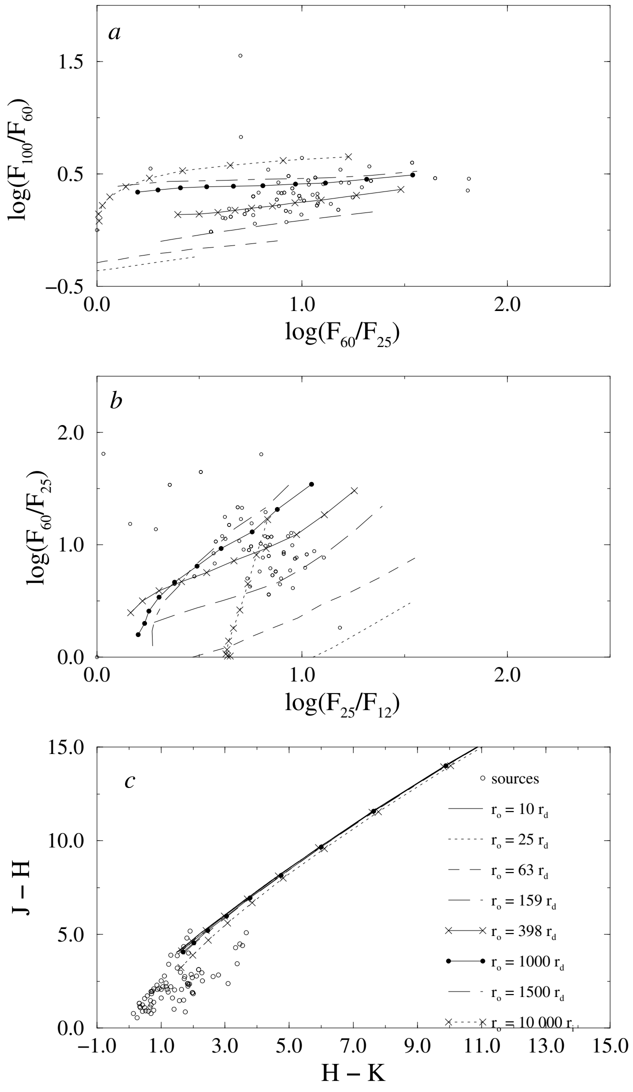

Figure 5. The effect of changing the outer radius. The central star has been set to spectral type O4 and the dust density distribution is constant. The dust destruction radius is $r_d = 1.27{\times}10^{14}$m.

radius which is kept fixed at the dust destruction radius, all the other parameters were the same as in Fig. 3. As in the case of Fig. 3 the predicted [100−60] colours are not very sensitive to the density gradient for the same reason as for the constant density case. Compared with the constant density case it is seen that the model predictions for the steeper density gradients have shifted towards the lower right on the [60−25] *vs* [25−12] two-colour diagram.

The NIR colours show no sensitivity to the change in density gradient. This is because the NIR emission is produced mostly at the inner edge of the cloud (see Fig. A2). In addition, the optical depth at the inner edge is the same for all cases and therefore the NIR emission has to propagate through the same amount of dust.

We finally show the case where the inner radius is kept fixed at the dust destruction radius but the outer radius is allowed to vary from 10 times the dust destruction radius to 10^4 times the dust destruction radius. The calculations are

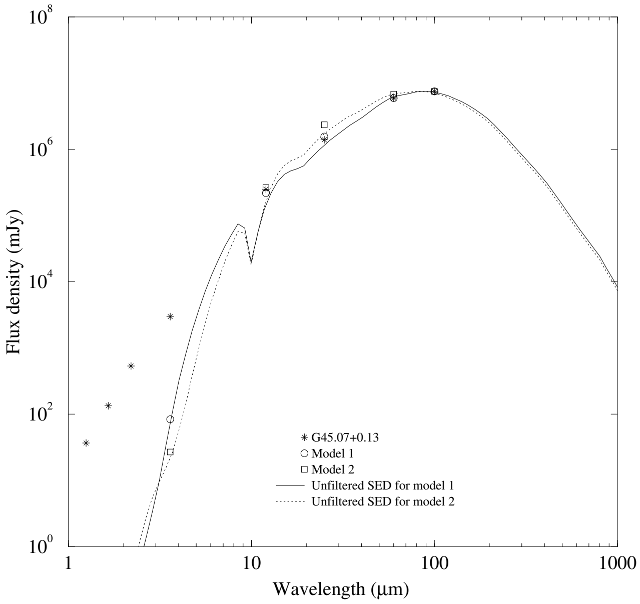

Figure 6. Model fits to the observations of the source G45.07+0.13. The SED is shown for two models as well as the fluxes obtained when the SED is convolved with the transmission functions for the filters.

for a constant radial dust density. The results are shown in Fig. 5.

Fig. 5a shows that the [100−60] colours are significantly more sensitive to changes in the outer radius than to changes in the inner radius. In this case the model results also bracket the observed results to a large extent. The reason for this behaviour is that the 100 and 60 μm emission comes predominantly from the outer parts of the cloud. Changing the outer radius from $10r_d$ to 10^4r_d drastically changes the temperature at the outer radius and therefore also the [100−60] colours. This result implies that the distribution of [100−60] colours may be a reflection of a distribution in cloud sizes. However, due to the number of other parameters that can be varied without affecting the [100−60] colours, it is not possible to estimate the cloud masses with any degree of confidence.

Fig. 5b shows that the observed range of [60−25] and [25−12] colours of the main group of sources can again be explained by the set of parameter values used in this case. Comparison with Figs. 3 and 4 suggest therefore that within the framework of a spherical model there is no unique set of parameter values that can explain the observed colours.

For the NIR colours it is seen in Fig. 5c that the model predictions cluster together with almost no overlap with the observed colours. This implies that the optical depths required to explain the observed NIR colours within the framework of the current model must be even smaller than 0.05 at 100 μm.

Using the knowledge gained in the parameter study, it is possible to vary the parameters in a systematic way to find the best fit to individual SEDs (if the SED is not inflected). Fig. 6 shows two model fits to the SED of a single source, G45.07+0.13 (*IRAS* 19111-1048). Table 2 gives the sets of parameters that were used to give the fits in Fig. 6. It was found that there is a large number of different combinations of parameters that can be used to give an acceptable fit. The spectral type of O5.5 was taken from the estimates of Wood & Churchwell (1989a). With the spectral type constrained, the values of the inner and outer radii are only dependent on the dust density distribution and the choice of optical depth.

It can be seen quite clearly in this figure that the models give very good fits to the *IRAS* fluxes but that shortward of the 9.7 μm feature the SED drops off very steeply, well below the observed NIR flux densities. Faison et al. (1998) also tried to fit the SED of this object using a spherically symmetric model. Even though their model includes small particles and could also fit the 9.7μm feature very well, it is clear that their model SED is also too steep between J and K-bands. In addition, their fit to the FIR part of the SED was not very good compared to their fit in the NIR region.

5 DISCUSSION

The most striking problem that comes up in the comparison between the observations and the model predictions is the fact that, from the point of view of the model, the observed NIR colours can only be produced at significantly smaller optical depths than the FIR colours. In the current data set there is not even one source for which the colours in the NIR and those in the FIR correspond to the same optical depth in the entire range of parameter values which we considered. This means that for all the sources in the data set the observed SEDs are flatter in the NIR, which implies higher NIR emission than that predicted by the model. The first obvious explanation of this discrepancy is that our dust model has only a single grain size and not a range of grain sizes that also includes small grains. The amount of NIR emission may be increased if the effects of very small, hot grains and polycyclic aromatic hydrocarbons (PAHs) are taken into account (Siebenmorgen 1993). These grains can reach higher temperatures than the grains modelled in this paper. However, Siebenmorgen (1993) had difficulty fitting the observations in the NIR, although the discrepancy is considerably less than that discussed here. He suggests that disk-like structures embedded in the circumstellar dust shell may resolve the problem. The same problem is noted by Efstathiou & Rowan-Robinson (1994).

The model presented here also neglects the effects of scattering. Since the scattering efficiency is proportional to λ^{-4} (Draine & Lee 1984), the effects of scattering will be more pronounced in the NIR than in the FIR. Although the inclusion of scattering may lead to an increase in flux at NIR wavelengths compared to our model results, it does not necessarily mean that the NIR colours will be bluer. This can be seen from an inspection of the results of eg. Efstathio & Rowan-Robinson (1990) and Churchwell et al. (1990). In these cases it is seen that although the fluxes are higher in the NIR relative to the observed fluxes than for our calculations, the SEDs are definitely steeper than the observed SEDs. It is therefore clear that there still is another factor that is being neglected in all models presented to date in order to explain the NIR part of the SEDs of massive star forming regions.

More recently Faison et al. (1998) tried to fit the SEDs of a number of UC HII regions using a spherical symmet-

Table 2. Parameters and derived cloud masses for the various fits to the observations of G45.07+0.13

Model no.	Spectral type	r_i (m)	r_o (m)	α	$\tau_{100\mu m}$	M_d $M_\odot$	M_{d+g} $M_\odot$
1	O5.5	1.368e15	1.914e16	0	0.16	222.2	3.920e4
2	O5.5	1.368e15	1.600e16	1	0.16	87.37	1.541e4

ric model. Although the calculated flux densities for these models are higher than ours when compared to the measured NIR flux densities, it is clear that most of their model SEDs are too steep in the NIR. In those cases where the NIR part of the SED is flatter, as eg. for G45.12+0.13, the fit in the FIR is very poor. However, for G45.12+0.13 the 9.7μm feature is barely visible implying a low optical depth at these wavelengths. The model SED for this source peaks at about 40 μm whereas the IRAS data suggests that the SED peaks at about 100 μm and most probably even beyond that. It follows therefore that the data suggest that the dust on the outer edges of the cloud is cooler than what is found in the model. Within the framework of a spherical symmetric model this means that the optical depth between the inner and outer edges of the cloud is too small, which gives rise to larger quantities of hot dust than suggested by the data. This case of G45.12+0.13 clearly illustrates that even with a sophisticated spherical symmetric model it is not possible to simultaneously fit the NIR and FIR parts of the observed SED. This is in qualitative agreement with what we found with our model.

A discrepancy similar to that described above for the maser sources and other UC HII regions also exists when the SEDs of lower mass stars in the Taurus-Auriga molecular cloud are compared with the predictions of spherically symmetric power-law density models. Kenyon et al. (1993) found that, compared to the model SEDs, the observed SEDs show NIR emission above levels that can be explained by spherically symmetric models. They also investigated the effect of axisymmetric density distributions (approximating circumstellar disks) and found that this not only increased the NIR emission significantly but also produced flatter SEDs in the NIR. A second peak, the strength of which is dependent on the inclination of the disk, is seen towards NIR wavelengths. This creates an effect which looks very similar to the inflection seen in some of the SEDs of the maser sources. It is possible therefore that a similar geometry is present in the maser sources.

We finally note that there are a number of sources which the model cannot fit between 12 and 60 μm. These are the sources that lie in the top left area of the $[60-25]$ *vs* $[25-12]$ two-colour diagrams. Clearly these cases need to be investigated further.

6 CONCLUSION

NIR photometry was carried out on 56 southern methanol maser sources. A spherically symmetric radiative transfer model of the surrounding dust cloud was developed in an attempt to understand the distribution of the sources on the two-colour diagrams. It was found that varying the different parameters can change the shape of different parts of the SED. However, there are still too many free variables to be able to model the maser sources using the infrared fluxes alone. Due to the scaling effect, additional information is needed on the spectral type of the central star and size of the cloud before individual sources can be modelled uniquely.

While the model can explain the FIR colours of the maser sources, it is not possible to fit the NIR colours with the same sets of parameters or vice-versa. The NIR colours imply significantly lower optical depths in the context of the model than the FIR colours. Such a difference cannot be explained by spherical symmetric models of embedded young massive stars. The discrepancy is too large to be entirely an artifact of the assumptions made in developing the model. It is clear that more sophisticated spherical symmetric models that use a range of particle sizes and include the effects of scattering are also not able to satisfactorily fit the observed infrared SEDs from the NIR to the FIR. We conclude that it is necessary to move away from spherical symmetric models if it is hoped to understand the infrared SEDs of the maser sources. Models which consider a circumstellar disk and outflows most probably have a better chance of reproducing the observed NIR characteristics of the maser sources.

APPENDIX A: THE MODEL

The dust cloud is assumed to be spherical with a dust-free central cavity which contains the embedded star and its HII region.

The dust grains were not modelled in detail. A single dust grain size was used ($a = 0.2\mu$m) with a composite emissivity function ϵ_ν (see Fig. A1) of silicate and graphite grains with sizes in the range 0.005–0.250 μm taken from the literature (Churchwell, Wolfire & Wood 1990). It has been shown (Efstathiou & Rowan-Robinson 1994) that composite grain models give results comparable to those of multigrain models. The transient heating of small grains, as described by Siebenmorgen et al. (1992) is also not treated.

Since the emergent radiation is emitted predominantly at FIR wavelengths and the scattering cross-section of dust grains is proportional to λ^{-4} (Draine & Lee 1984), we assume that the effects of scattering can be ignored. However, scattering will be important in the innermost regions of the cloud where the radiation is still predominantly at short wavelengths.

The temperature of the dust grains as a function of the distance from the central star can be found by requiring that the grains be in thermal equilibrium. Thus the energy radiated by the individual dust grains is equal to the energy absorbed by these grains:

$$W^{+}_{star}(r) + W^{+}_{dust}(r) = W^{-}(r) \quad \text{(A1)}$$

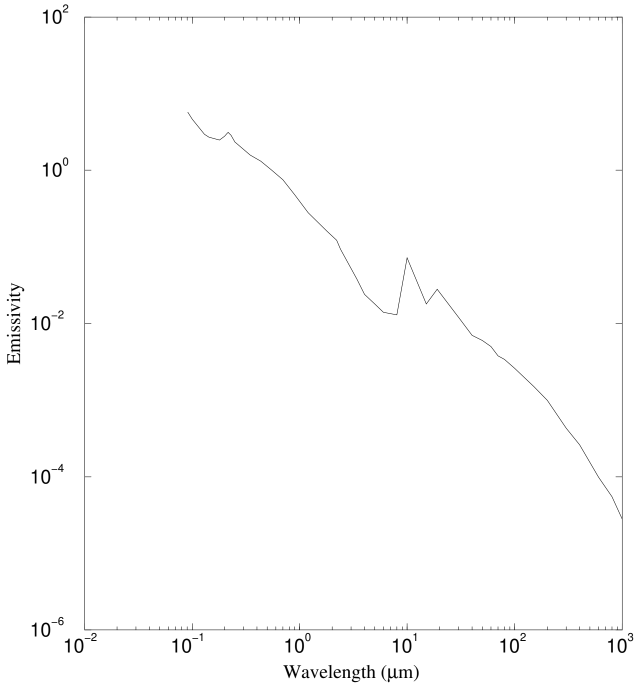

Figure A1. Emissivity function used in the parameter study.

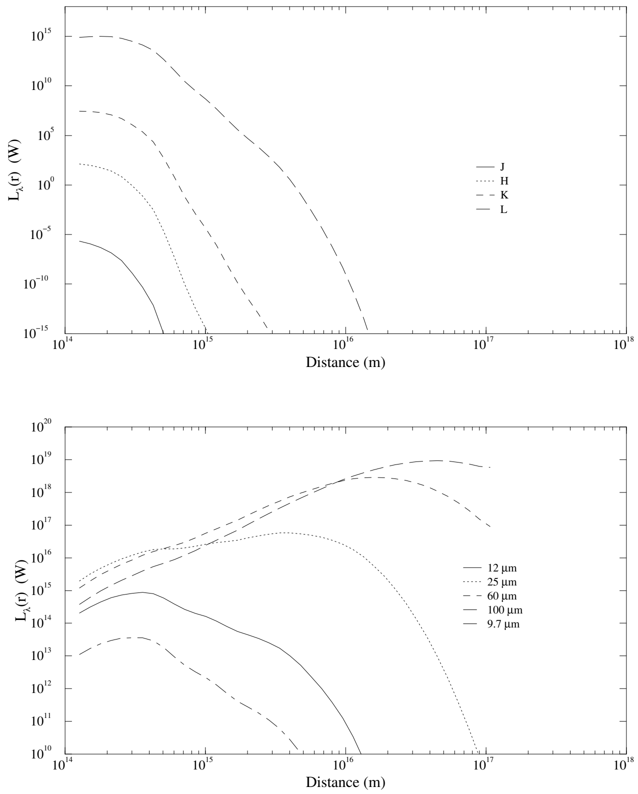

Figure A2. The origin of the emergent radiation for a cloud with constant dust density, $\tau_{100\mu m} = 0.5$ and central star of spectral type O4. The strength of the radiation at the given wavelengths which reaches the outside of the cloud after being emitted from a thin shell at r is shown. In this high optical depth case the NIR radiation is so strongly attenuated that it is more than 10 orders of magnitude weaker than the FIR radiation

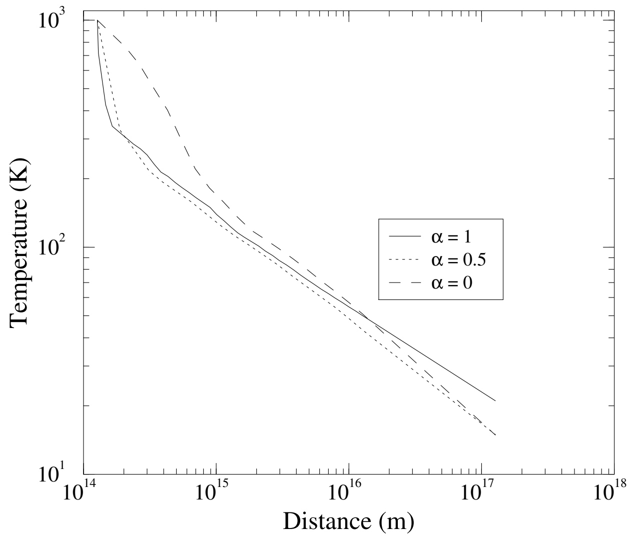

Figure A3. Temperature profiles for clouds with different dust density gradients. The central star has been set to O4 and $\tau_{100\mu m} = 0.5$

The power absorbed by the dust grain from stellar radiation is given by

$$W^+_{star}(r) = \int_0^\infty d\nu \, \frac{L_\nu}{4\pi r^2} \pi a^2 Q_{abs}(\nu) e^{-\tau_\nu}. \quad \text{(A2)}$$

The power absorbed by a dust grain from radiation from other dust grains is

$$W^+_{dust}(r) = \int_{r_i}^{r_o} dr' \, n_d(r')(r')^2 \int_0^{2\pi} d\phi \int_0^\pi d\theta \; \sin\theta \beta(r', \theta), \quad \text{(A3)}$$

where

$$\beta(r', \theta) = \int_0^\infty d\nu \, \pi B_\nu[T_d(r)] \frac{a^2}{l^2} \pi a^2 Q^2_{abs}(\nu) \; \exp\left[- \int_0^l dl' \, n_d(r'') \pi a^2 Q_{abs}(\nu) \right]. \quad \text{(A4)}$$

The power radiated by the dust grain is given by

$$W^-(r) = \int_0^\infty d\nu \, 4\pi a^2 Q_{abs}(\nu) \pi B_\nu(T_d). \quad \text{(A5)}$$

The temperature gradient across the dust cloud turns out to be quite complex and cannot easily be described using a single function. Instead, the dust cloud is divided into a number of shells such that the temperature gradient follows a power law in each shell and follows smoothly from the previous shell:

$$T(r) = T(r_{j-1}) \left(\frac{r_{j-1}}{r} \right)^{\gamma_j}, \quad \text{(A6)}$$

where $r_{j-1} < r \leq r_j$, r_j is the outer boundary of the jth shell and $T(r_{j-1})$ is the dust temperature at the outer edge of the previous shell.

A method using converging approximations, which eliminates the need for an initial guess, was used to find $T(r)$ by solving equation A1. The method works as follows:

- Set T_0 to the dust destruction temperature if the inner radius has been set to the dust destruction radius. Start at the innermost shell and take into account only heating from the central star and dust grains within that shell i.e. ignore the outer part of the dust cloud when evaluating equation A3.

- Solve for γ_1 using a simple bisection method to solve the equation of energy balance (equation A1).
- Move to the next shell and solve for γ_2 taking into account heating from dust in the previous shell as well, but ignore the outer part of the dust cloud.
- Continue in this manner until the temperature gradient is found in all shells. Now $T_d(r)$ exists for all r.
- Repeat the above steps but this time take into account heating due to dust from the entire cloud i.e. evaluate equation A3 for all r. The procedure is repeated until the solution converges to a predetermined tolerance (5%).

Once the temperature gradient has been found, the emergent SED can be found by tracing light paths through the cloud.

Figure A2 shows the regions of the cloud in which the radiation of different wavelengths is predominantly produced. It can be seen that the NIR radiation is produced by the hot dust near the inner edge of the cloud. The NIR radiation is also strongly attenuated by the dust in the outer parts of the cloud. The FIR emission, especially the 60 μm and 100 μm radiation, is produced mostly by the cold dust at the other edges of the cloud. This behaviour is to be expected.

The model was checked by comparing the results with those of other researchers. It was found that the shape of the temperature gradient (see Figure A3) is the same as that found by Efstathiou & Rowan-Robinson (1994) and Wolfire and Cassinelli (1994). The temperature gradients were found to scale with the luminosity of the central star. This effect has also been noted previously (Rowan-Robinson 1980; Ivezić & Elitzur 1997).

The model is also self-consistent. Since the temperature gradient was calculated by imposing conservation of energy, the solution was deemed to be satisfactory when the emergent luminosity was equal to the bolometric luminosity of the central star. In most cases there was a deviation of less than 5 % from luminosity conservation. Only the cases with steep dust density gradients ($\alpha = 1$) had a problem, with the deviation from luminosity conservation being between 10–30%.

REFERENCES

Adams, F.C., Shu, F.H., 1985, ApJ, 296, 655
Caswell, J.L., Vaile, R.A., Ellingsen, S.P., Whiteoak, J.B., Norris, R.P., 1995, MNRAS, 272, 96
Caswell, J.L., 1996, MNRAS, 279, 79
Caswell, J.L., 1997, MNRAS, 289, 203
Churchwell, E., 1990, A&AR, 2, 79
Churchwell, E., Wolfire, M.G., Wood, D.O.S., 1990, ApJ, 354, 247
Crawford, J., Rowan-Robinson, M., 1986, MNRAS, 221, 923
Draine, B. T., Lee, Hyung Mok, 1984, ApJ, 285, 89
Efstathiou, A., Rowan-Robinson, M., 1990, MNRAS, 245, 275
Efstathiou, A., Rowan-Robinson, M., 1994, MNRAS, 266, 212
Faison, M., Churchwell, E., et al., 1998, ApJ, 500, 280
Hunter, T.R., Phillips, T.R., Menten, K.M., 1997, ApJ, 478, 283
IRAS Point Source Catalogue, 1985, *IRAS* Science Working Group, US Government Printing Office, Washington, DC
Ivezić, Ž., Elitzur, M., 1997, MNRAS, 287, 799
Kenyon, S.J., Calvert, N., Hartman, L., 1993, ApJ, 414, 676
Kessel, O., Yorke, H.W., Richling, S., 1998, A&A, 337, 832
Kurtz, S., Churchwell, E., Wood, D.O.S., 1994, ApJS, 91, 659
Leitherer, C., Robert, C., Drissen, L., 1992, ApJ, 401, 596
MacLeod, G.C., Gaylard, M.J., Nicolson, G.D., 1992, MNRAS, 254, 1p
MacLeod, G.C., Gaylard, M.J., 1992, MNRAS, 256, 519
Menten, K.M., 1991, ApJ, 380, L75
Minier, V., Booth, R.S., Conway, J.E., 1998, A&A, 336, L5
Norris, R.P. et al., 1998, ApJ, 508, 275
Panagia, N., 1973, AJ, 78, 929
Phillips, C.J., Norris, R.P., Ellingsen, S.P., McCulloch, P.M., 1998, MNRAS, 300, 1131
Rowan-Robinson, M., 1980, ApJS, 44, 403
Schutte, A.J., van der Walt, D.J., Gaylard, M.J., MacLeod, G.C., 1993, MNRAS, 261, 783
Scoville, N., Kwan, J., 1976, ApJ, 206, 718
Siebenmorgen, R., 1993, ApJ, 408, 229
Siebenmorgen, R., Krügel, E., Mathis, J.S., 1992, A&A, 266, 501
Tielens, A.G.G.M., de Jong, T., 1979, A&A, 75, 326
van der Walt, D.J., Gaylard, M.J., MacLeod, G.C., 1995, A&AS, 110, 81
Wolfire, M.G., Cassinelli, J.P., 1986, ApJ, 310, 207
Wolfire, M.G., Churchwell, E., 1994, ApJ, 427, 889
Wood, D.O.S., Churchwell, E., 1989a, ApJS, 69, 831
Wood, D.O.S., Churchwell, E., 1989b, ApJ, 340, 265
Yorke, H.W., 1980, A&A, 86, 286
York, H.W., Bodenheimer, P., Laughlin, G., 1995, ApJ, 443, 199

ACKNOWLEDGEMENTS

We would like to thank Mike Gaylard and Beate Woermann for their helpful comments and suggestions.